PROPAGATION AND SECONDARY PRODUCTION OF LOW ENERGY ANTIPROTONS IN THE ATMOSPHERE*

T. Bowen and A. Moats
Department of Physics
University of Arizona, Tucson, AZ 85721, USA

1. Introduction. Current theories, in which the observed antiproton component is attributed strictly to secondary production in high energy inelastic collisions of protons with the interstellar medium or the atmosphere, apparently fail to explain the relatively high $\bar{p}$ vertical intensities measured at mountain and balloon altitudes. Therefore, a more careful calculation of the theoretical secondary intensity spectra is required before more exotic sources for these excess $\bar{p}$'s can be explored.

In this paper, we have used a one-dimensional diffusion equation (valid if $\theta_{lab} \leq 20^{0}$ down to sea level) to calculate the expected vertical intensity of $\bar{p}$'s due only to secondary production in the atmosphere; any assumed primary $\bar{p}$ spectrum can also be included. Two adjustable parameters, the inelasticity and charge exchange in nucleon-nucleus collisions, were included in our algorithm. In order to obtain an independent estimate of their values, we first calculated the proton vertical intensities in the atmosphere, adjusting the parameters until our curves fit the experimental proton data, and then assumed that these values were identical in antinucleon-nucleus collisions.

2. Results. Our calculations followed a method suggested to us by T. K. Gaisser in which the atmosphere was divided into "slabs" of equal thickness Δx; slabs of 1 g/cm^2 were used. In calculating the differential proton intensities, a primary proton spectrum of the form[1] $j_p = 2(E + 2.15)^{-2.75}$ cm^{-2}-s^{-1}-sr^{-1}-GeV^{-1}, where E is the proton kinetic energy in GeV, was assumed. Protons and neutrons from higher Z nuclei were assumed to have the same spectral shape, and all protons and nuclei whose momenta were less than the vertical cutoff rigidity were excluded. Then, working from the top of the atmosphere down to sea level, the proton intensity of the i + 1 slab was calculated using the equations n(i + 1) = n(i) + (dn(E)/dx)Δx and

$$\frac{dn_p(E)}{dx} = -\frac{n_p(E)}{\lambda^{air}_{inel}} + \left(\frac{dE}{dx}\right)\frac{\Delta n_p}{\Delta E} + \int_{E_0=E}^{\infty} \frac{1}{\lambda^{air}_{inel}} \frac{dN(E,E_0)}{dE} [(1-\alpha)n_p(E_0) + \alpha n_n(E_0)]dE_0 \, , \quad (1)$$

with a similar equation [without the ionization loss[2] term $(dE/dx)(\Delta n_p/\Delta E)$] for the neutron intensity, n_n. All of the values of n on the right-hand side are the values from the slab i above. λ^{air}_{inel} is the inelastic mean-free path of proton-air nuclei collisions, scaled from p-^{12}C data.[3,4] The last term in the equation above adds in the protons gained from inelastic collisions of higher energy protons with air nuclei, with $dN(E,E_0)/dE$ defined as the probability of a proton with initial energy E_0 possessing energy E after collision. A uniform probability distribution ranging from 0 to εE_0 for $dN(E,E_0)/dE$, with average elasticity $\varepsilon/2$, was assumed. ε and the probability α of charge exchange were our adjustable parameters. With the values α = 0.333 and ε = 0.9, our computed proton intensities matched the experimental data quite well (see Fig. 1). We then used these values for ε and α in our antiproton intensity calculations.

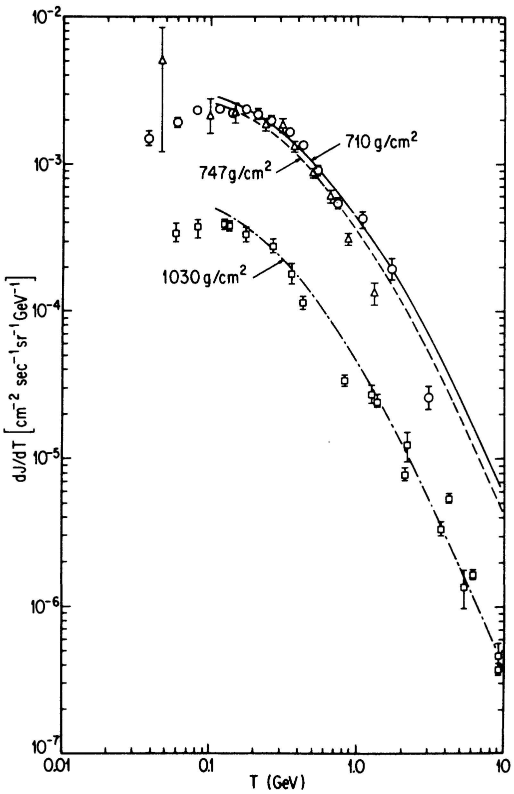

Fig. 1. The curves show the calculated results for vertical proton intensities at 710, 747, and 1030 g/cm^2 depth. The data is a compilation by Barber et al., Ref. 14.

Using the same method, the antiproton intensity due only to secondary production was calculated with equations analogous to Eq. (1), but with the term,

$$\int_{E_0=E}^{\infty} \frac{1}{\lambda^{air}_{inel}} \frac{1}{\sigma^{air}_{inel}} \frac{d\sigma^{air}_{\bar{p}}(E,E_0)}{dE} n_{nucleon}(E_0)dE_0 \quad ,$$

added on the right side for the production spectrum of $\bar{p}$'s in proton-air collisions, which is taken from a parameterization of Tan and Ng,[5] attenuated with an attenuation length of 122 g/cm^2 as depth increases. The form of dE/dx and dN(E,E$_0$)/dE were the same as used in the proton calculations. $\bar{\lambda}^{air}_{R}$, the $\bar{p}$ mean-free path in air for annihilation and inelastic scattering, was estimated by scaling a power-law fit to $\bar{p}$-^{12}C reaction cross sections from data compiled by G. Bruge[6] and provided to us by J. C. Peng, LAMPF; the result is shown in Fig. 2, curve d, along with another estimate,[7] curve e. Three different forms of $\bar{\lambda}^{air}_{inel}$, the antiproton mean-free path in air for inelastic, non-annihilation collisions, were tried, as shown in Fig. 2. In version c, $\bar{\lambda}^{air}_{inel}$ was assumed to be equal to λ^{air}_{inel} for protons. A curve from Szabelski and Wolfendale[7] was used in version b. Finally, in version a, we attempted a realistic estimate for $\bar{\lambda}^{air}_{inel}$ by assuming that $\bar{\lambda}^{air}_{inel}$ / $\bar{\lambda}^{air}_{annih}$ = $\sigma_{annih}(\bar{p}p)/\sigma_{inel}(\bar{p}p)$. Since there is little data available on $\sigma_{inel}(\bar{p}p)$ [non-annihilation], we assumed that it is the same as the pp inelastic cross section.[8] Below 0.5 GeV, $\bar{\lambda}^{air}_{inel}$ depends entirely on quasi-elastic $\bar{p}$-nucleon scattering; for our realistic estimate shown in curve a, the quasi-elastic scattering was taken to be 1/10 as probable as for the p-nucleon case, based upon special Monte Carlo runs using ISABEL INC for $\bar{p}$-^{12}C inelastic scattering at 180 and 400 MeV[9] arranged for us by P. L. McGanghey at Los Alamos.

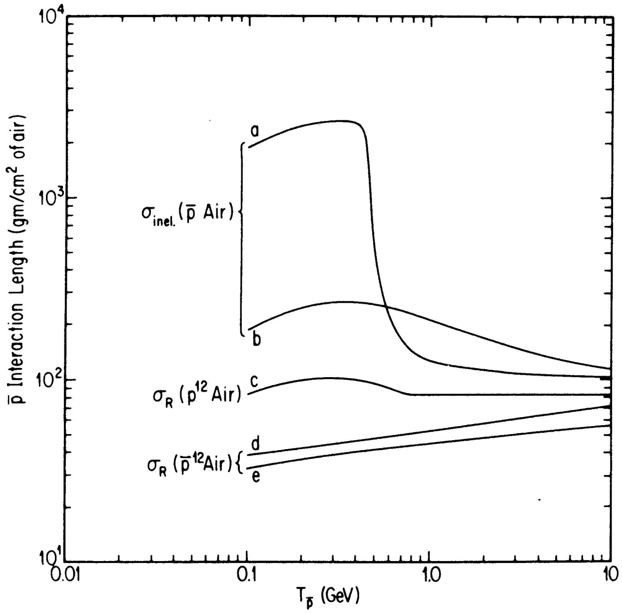

Fig. 2. Antiproton-air interaction lengths (mean-free paths) employed in the calculations: (a) $\bar{\lambda}^{air}_{inel}$ derived from our most realistic estimate of $\sigma_{inel}(\bar{p}\text{-air})$; (b) $\bar{\lambda}^{air}_{inel}$ from Ref. 7; (c) $\bar{\lambda}^{air}_{inel}$ derived if $\sigma_{inel}(\bar{p}\text{-air}) = \sigma_R(p\text{-air})$; (d) $\bar{\lambda}^{air}_R$ derived from our fit to $\sigma_R(\bar{p}\text{-}^{12}C)$ data; (e) $\bar{\lambda}^{air}_R$ from Ref. 7.

The results of our antiproton calculations, along with experimental data for the $\bar{p}$ vertical intensities at mountain altitudes, are shown in Fig. 3. At mountain altitude, both curves a and c are consistent with observations by the Arizona group,[10] although we feel that the comparison with curve a, our most realistic estimate, is the more significant one. At balloon altitudes, our secondary $\bar{p}$ intensity estimates are an order of magnitude below the intensities reported by Buffington et al.[11] and Golden et al.[12]

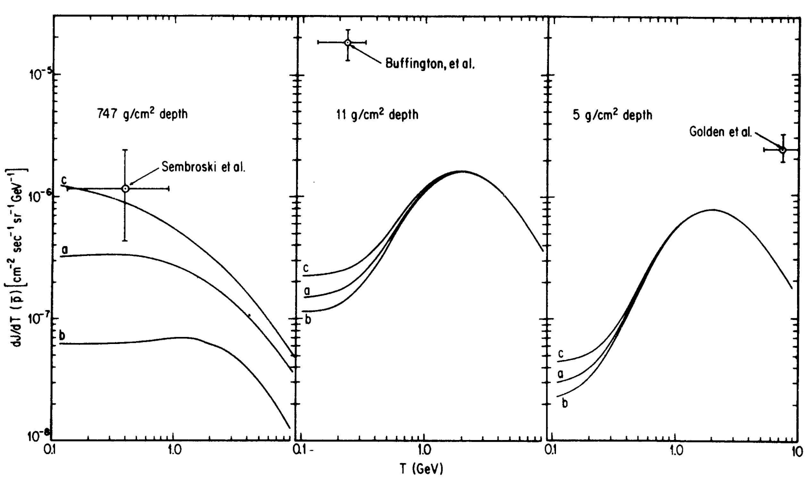

Fig. 3. The curves show calculated antiproton intensities produced by atmospheric interactions at 747 g/cm^2 11 g/cm^2, and 5 g/cm^2 depth. The data points are taken from Refs. 10, 11, and 12. The designations (a), (b), and (c) correspond to utilizing curves (a,d), (b,e), and (c,d), respectively, from Fig. 2.

These results assume that there is no primary $\bar{p}$ spectrum. We then added to version "a" a primary $\bar{p}$ spectrum normalized by passing through the point of Golden et al.[12] at 8.5 GeV of the form $j_{\bar{p}}=(2.4\times10^{-6})[(E+0.94)/9.44]^{-\gamma}$. If γ=2.75 as for the proton spectrum, then the resultant low energy spectrum at mountain altitude (747 g/cm^2) was 2.0% greater than the purely secondary $\bar{p}$ spectrum; with γ=2.1 as suggested by Stecker and Wolfendale,[13] the primary $\bar{p}$ contribution at mountain altitude increases to 4.8%. Then γ was adjusted until the calculated low energy $\bar{p}$ intensity at 747 g/cm^2, due to the primaries, equaled the difference between the data from Bowen et al.[10] and the calculated result for purely secondary $\bar{p}$ spectrum [Fig. 3(747 g/cm^2), curve a]. A rather flat spectrum, γ=0.95, is required. We also determined the most probable energy of the primary antiprotons contributing to the low energy $\bar{p}$'s at 747 g/cm^2: for γ=2.1, it was 30 GeV; for γ=1.5, 240 GeV; for γ=0.9, 3800 GeV. Obviously, more data on the antiproton intensities at high altitudes, as well as additional data on $\bar{p}$ cross sections, are needed before making an analysis with fewer approximations.

*This work was supported by NSF Grant PHY-82-07697.

1. Compilation presented by D. Müller, Proceedings of Workshop on Very High Energy Cosmic Ray Interactions, Philadelphia, April 22-24, 1982, p. 448.
2. "Review of Particle Properties," Revs. Mod. Phys. 56, No. 2, Part II, p. S49 (April 1984).
3. Compilation by N. J. DiGiacomo et al., Phys. Rev. Lett. 45, 527 (1980).
4. G. Bellettini et al., Nucl. Phys. 79, 609 (1966).
5. L. C. Tan and L. K. Ng, J. Phys. G: Nucl. Phys. 9, 227 (1983). We used the parameterization for the "Stephens spectrum" multiplied by 1.43 to account for nuclei with Z > 1 and by 0.71 for shadowing of air nucleons when comparing equal g/cm^2 of air and hydrogen targets.
6. Compilation presented by G. Bruge, Symp. on Nuclear Spectroscopy and Nuclear Interactions, Osaka, March 21-24, 1984 (Report D Ph-N-Saclay No. 2136) of PS184 collaboration results along with earlier results compiled in K. Nakamura et al., Phys. Rev. Lett. 52, 731 (1984).
7. J. Szabelski and A. W. Wolfendale (private communication).
8. V. Flaminio et al., "Compilation of Cross Sections III: p and $\bar{p}$ Induced Reactions, CERN-HERA 84-01 (17 Apr. 1984).
9. M. R. Clover et al., Phys. Rev. C 26, 2138 (1982); M. R. Clover, P. L. McGaughey, and Y. Yariv (private communication).
10. T. Bowen, E. W. Jenkins, J. J. Jones, A. E. Pifer, and G. H. Sembroski, Papers of 18th Int. Cosmic Ray Conf., Bangalore, Aug. 22-Sept. 3, 1983, vol. 2, p. 96.
11. A. Buffington et al., Astrophys. J. 248, 1179 (1981).
12. R. L. Golden et al., Phys. Rev. Lett. 43, 1196 (1979).
13. F. W. Stecker and A. W. Wolfendale, Nature 309, 37 (1984).
14. H. B. Barber et al., Phys. Rev. D 22, 2667 (1980).